$$\alpha_W = (2)^{1/2}\frac{\omega}{c}\left\{-\left(1-\frac{\omega_c^2}{\omega^2}-\frac{(\omega_p/\omega)^2}{1+(\nu/\omega)^2}\right)+\left[\left(1-\frac{\omega_c^2}{\omega^2}-\frac{(\omega_p/\omega)^2}{1+(\nu/\omega)^2}\right)^2+\left(\frac{\nu/\omega(\omega_p/\omega)^2}{1+(\nu/\omega)^2}\right)^2\right]^{1/2}\right\}^{1/2} \quad (4)$$

where ω_c is the waveguide mode cutoff frequency in the absence of plasma, and the rest of the parameters have been defined earlier.

The curves comparing the salient features of the plasma absorption per unit length (α_H and α_W) for the two Aro-Walsh experiments are shown in Fig. 2. It is seen that, as far as the measuring system is concerned, the major effect of the waveguide boundary condition is an apparent increase in the electron plasma density. In other words, the measuring system essentially cannot tell whether a waveguide boundary has been imposed on the plasma or whether the plasma density has in fact increased. Thus, it would not be meaningful to compare the two experimental curves for electron temperature (of Fig. 1) on a one-to-one basis but allowance must first be made for a shift in the general features of the waveguide probe results toward lower actual plasma densities or shock levels.

For the 9.05-GHz center frequency considered here, the critical plasma density is about 10^{18} m^{-3}, yielding a "knee" in the absorption curve for the microwave-horn experiment at about Mach 7.1 (Fig. 2); whereas in the waveguide probe experiment, the knee in the absorption curve is at about Mach 6.95, corresponding to a virtual critical density of about 3.5×10^{17} m^{-3} (Fig. 2), or about a factor of three lower. In the microwave-horn experiment the electron plasma temperatures exceed the theoretical values between Mach 6.8 and 7.4, corresponding to plasma densities between about 1.5×10^{17} and 4×10^{18} m^{-3}, or between about 0.15 and 4 times the critical density. Thus, if the results of the waveguide probe experiment were to exhibit the same type of anomalous form at relatively low densities, we would expect it to occur between about 0.15 and 4 times the *virtual* critical density (for this case 3.5×10^{17} m^{-3}), corresponding to shock levels between Mach 6.6 and 7.2. However, as discussed earlier, the electron temperature could not be computed below Mach 7.3 in the waveguide probe experiment due to a basic shortcoming in the technique itself. Therefore, the anomalous results in the lower Mach region of the microwave-horn experiment remain unexplained.

References

[1] Peperone, S. J., "X-Band Measurement of Shock-Tube Plasma Temperature," *Journal of Applied Physics*, Vol. 33, No. 2, Feb. 1962, p. 767.

[2] Gerardo, J. B., Goldstein, L., and Hendricks, C. D., Jr., "Application of Microwaves in Shock Wave Investigations," *Proceedings of the Sixth International Conference on Phenomena of Ionized Gases*, Vol. 4, 1963, pp. 331–338.

[3] Aro, T. O. and Walsh, D., "Attempted Microwave Measurement of Temperature of a Shock-Heated Plasma," *The Physics of Fluids*, Vol. 10, No. 7, July 1967, pp. 1468–1476.

[4] Aro, T. O. and Walsh, D., "Measurement of Plasma Temperature Using a Waveguide Probe," *The Physics of Fluids*, Vol. 11, No. 5, May 1968, pp. 1070–1075.

[5] Singer, A. and Minkowski, J. M., "Determination of Electron Temperature of Shock-Heated Plasma from Microwave Measurements," *The Physics of Fluids*, Vol. 16, No. 7, July 1973, pp. 1176–1177.

[6] Singer, A. and Minkowski, J. M., "Suitability of the Waveguide Probe Technique for Measuring Electron Plasma Temperature," *The Physics of Fluids*, Vol. 16, No. 11, Nov. 1973, pp. 2038–2039.

[7] Bekefi, G. and Brown, S. C., "Emission of Radio-Frequency Waves from Plasmas," *American Journal of Physics*, Vol. 29, No. 7, July 1961, pp. 404–428.

[8] Wharton, C. B., "Microwave Techniques," *Plasma Diagnostic Techniques*, edited by R. H. Huddlestone and S. L. Leonard, Academic Press, New York, 1965, pp. 477–499.

[9] Tanenbaum, B. S., *Plasma Physics*, McGraw-Hill, New York, 1967, p. 252.

[10] Heald, M. A. and Wharton, C. B., *Plasma Diagnostics with Microwaves*, Wiley, New York, 1965, p. 165.

Wall Shear and Boundary-Layer Measurements in Shock Separated Flow

PAUL J. WALTRUP* AND JAMES M. CAMERON†

The Johns Hopkins University, Silver Spring, Md.

IN Ref. 1, the instream flow structure of a nonreacting supersonic flow in a cylindrical duct containing a stabilized shock system was described and an empirical correlation for the resulting wall static pressure distribution [$p_w(s)$] and distance over which the shock pressure rise spreads (s_t) presented. These relationships, in turn, were used to predict the precombustion shock wall pressure distribution in a scramjet engine[2] since the two flows are analogous. Although these reports presented a reasonably accurate description of the over-all instream wave structure, they left to conjecture its interaction with the wall boundary-layer. This Note presents wall shear and boundary-layer pitot pressure measurements that permit a more precise definition of the flow at and near the wall in the interaction region and serve as a check on the theoretically derived turbulent boundary-layer properties used in the empirical correlation. These, in turn, allow a complete depiction of the instream and wall flow structure in a shock separated flow of this type.

Experiments

Figure 1 presents a schematic of the test apparatus, instrumentation, and flow structure generated. In each test, ambient temperature ($T_{t_0} \cong 520°R$) air is passed through a Mach 2.65 (M_a) nozzle into a 2.74-in.-diam cylindrical duct, 16.69 in. long, and discharged to the atmosphere. By lowering the tunnel total pressure (p_{t_0}), overexpanded flows are generated which create shock structures within the cylindrical test section of sufficient strength to raise the initial pressure (p_a) to the exhaust (or back) pressure (p_f). This is denoted as the shock/boundary-layer interaction region in Fig. 1 and extends over the distance s_t. Measurements of wall shear (τ_w) and boundary-layer pitot pressure (p_t') were taken in and upstream of this region at the axial stations indicated in Fig. 1 along with wall static pressures at approximately one inch intervals. Boundary-layer pitot pressure profiles were measured using two pitot rakes positioned 90° apart circumferentially for redundancy and all pressures were

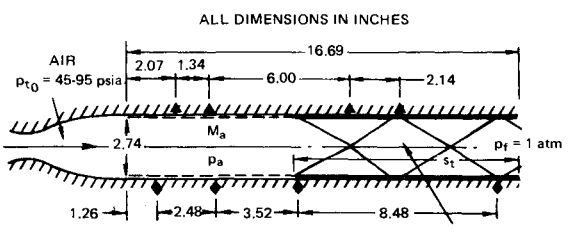

Fig. 1 Schematic of test set-up, instrumentation, and flow structure.

Received January 11, 1974. This work was supported by the United States Navy under Naval Ordnance Systems Command Contract N00017-72-C-4401.

Index categories: Nozzle and Channel Flow; Shock Waves and Detonations; Boundary Layers and Convective Heat Transfer—Turbulent.

* Section Supervisor, Supersonic Combustion, Applied Physics Lab. Member AIAA.

† Engineering Staff Associate, Propulsion Research Laboratory, Applied Physics Lab.

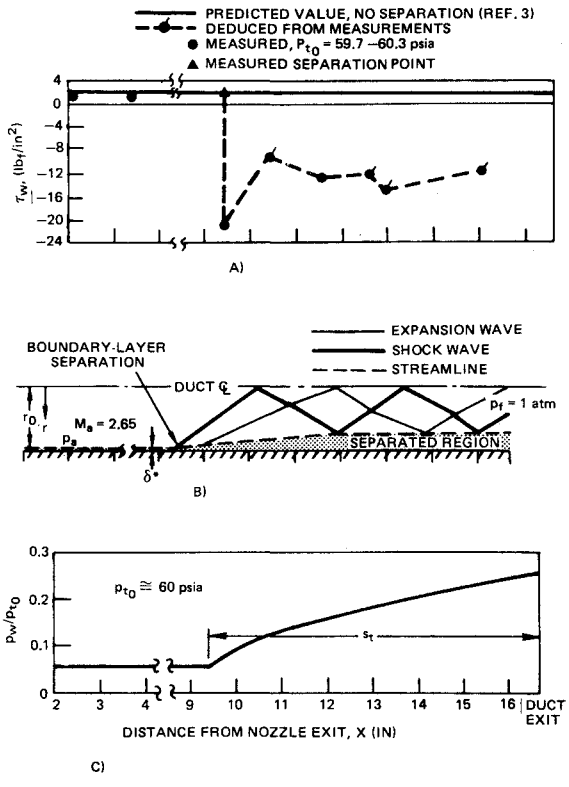

Fig. 2 a) Wall shear stress, b) flow structure, and c) wall static pressure distribution in overexpanded supersonic duct flow.

deduced via straingage transducers (±0.5% full-scale error). Wall shear was measured using a JHU/APL designed floating-head, strain-sensing skin-friction balance. Briefly, this consists of a circular button (area = 0.1356 in.^{2}), contoured to match the duct curvature, which sits flush with the duct surface and is attached to a cantilevered beam rigidly fastened to the balanced housing. The beam has two p-type silicone semiconductor crystals (strain sensors) rigidly attached 180° apart and is contoured to provide a uniform stress along each of the crystal elements. Both crystals are aligned normal to the axis of rotation and measure only axial strain. Accuracy and repeatability of the balance over a ±15 g (±0.033 lbf) loading range is ±0.5% on a 10 mv full-scale range. Although measurements were made for $45 = p_{t_0} = 95$ psia, for brevity, only those for $p_{t_0} \cong 60$ psia are presented below.

Experimental Results and Conclusions

Figure 2a presents the measured values of wall shear for $p_{t_0} \cong 60$ psia and compares them to the theoretically predicted

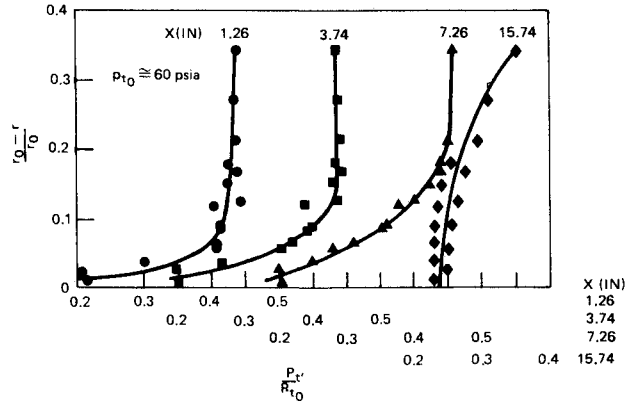

Fig. 3 Boundary-layer pitot pressure profiles for $P_{t_0} \cong 60$ psia.

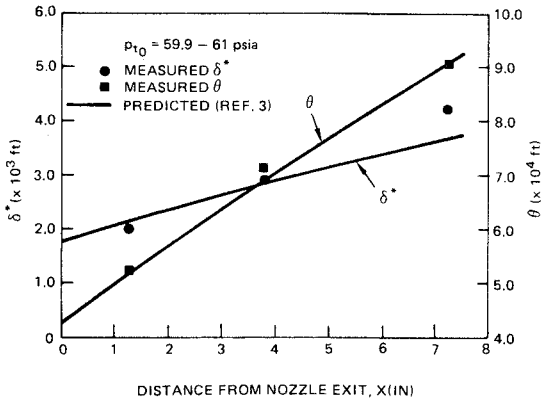

Fig. 4 Comparison of measured and predicted values of boundary-layer displacement (δ^*) and momentum (θ) thickness.

values for a turbulent unseparated flow using the momentum integral technique of Ref. 3. Agreement with the measured values (solid symbols) is good at $x = 2.07$ in. (0.0185 vs 0.0173 lbf/in.^{2}) but poorer at $x = 3.41$ in. (0.0181 vs 0.0123 lbf/in.^{2}), indicating that the actual wall shear is decreasing faster than theoretically predicted. Figure 2a also shows that the boundary layer separates at the initiation of the shock structure and remains separated throughout the entire interaction region. Figure 2b presents the final analytical model of the interaction region based on the in-stream wave structure presented in Ref. 1 and the wall shear measurements of Fig. 2a. The incoming flow (M_a, p_a) is subjected to a series of oblique shock and expansion waves and their reflections from the duct centerline until the pressure is raised to p_f. The initial shock wave separates the boundary layer, which remains separated throughout the interaction region. Because each wave depicted in Fig. 2b actually comprises a multiplicity of waves, continuous, rather than abrupt, changes are observed in the normalized wall static pressure (p_w/p_{t_0}) as indicated in Fig. 2c and the axial instream pitot pressure profiles shown in Ref. 1. On the other hand, the wall shear measurements in Fig. 2a do indicate local variations in the magnitude of flow reversal of the separated boundary layer. The largest negative wall shear occurs behind the initial oblique shock, which is the strongest of the compression waves present and the smallest negative wall shear occurs just behind the first (strongest) expansion wave. This same trend is also apparent for the intersections at the wall of the centerline reflection of the initial shock and expansion waves. The dashed line in Fig. 2a was obtained by positioning the skin-friction balance at $x = 11.55$ in. and then operating with different degrees of overexpansion (i.e., different p_f/p_a), measuring the wall shear and shifting the abscissa according to the following knowledge and reasoning. Previous work[1] has shown that for p_f/p_a lower than the maximum value permissible to keep the tunnel from unstarting, the wave structure for a lower value of p_f/p_a is just a proportional part of the wave structure present in the maximum case, and the location of the origin of the wave structure is directly related to p_f/p_a. Thus, the measured value of wall shear for a different value of p_w/p_a just corresponds to the shear that would be present at a different location.

Figure 3 presents boundary-layer pitot pressure profiles at the four stations indicated in Fig. 1 for $p_{t_0} \cong 60$ psia. The growth of the boundary layer with axial distance in the unseparated region is readily apparent, and the separated profile at $x = 15.74$ in. is characterized by nearly constant pitot pressure near the wall followed by increasing pressure, indicative of the free (or separated) shear layer. In Fig. 4, the unseparated pitot pressure profiles in Fig. 3 have been used to calculate local values of displacement thickness (δ^*) and momentum thickness (θ) assuming the static pressure (p_w) and total temperature (T_{t_0}) to be radially constant. In each case, the measured values of δ^* and θ have been corrected for pitot probe interference effects as

detailed in Ref. 4. These, in turn, are compared to the values theoretically predicted by the method of Ref. 3. The agreement achieved is excellent and confirms the validity of the theoretical values of boundary-layer properties used in the empirical correlation of Ref. 1.

References

[1] Waltrup, P. J. and Billig, F. S., "The Structure of Shock Waves in Cylindrical Ducts," *AIAA Journal*, Vol. 11, No. 10, Oct. 1973, pp. 1404–1408.

[2] Waltrup, P. J. and Billig, F. S., "Prediction of Precombustion Wall Pressure Distributions in Scramjet Engines," *Journal of Spacecraft and Rockets*, Vol. 10, No. 4, Sept. 1973, pp. 620–622.

[3] Glowacki, W. J., "Fortran IV (IBM 7090) Program for the Design of Contoured Axisymmetric Nozzles for High Temperature Air," NOLTR 64-219, Feb. 1965, U.S. Naval Ordnance Lab., White Oak, Silver Spring, Md.

[4] Allen, J. M., "Impact-Probe Displacement in a Supersonic Turbulent Boundary-Layer," *AIAA Journal*, Vol. 10, No. 4, April 1972, pp. 555–557.